# ICESat observations of seasonal and interannual variations of sea-ice freeboard and estimated thickness in the Weddell Sea, Antarctica (2003–2009)

Donghui YI,[1] H. Jay ZWALLY,[2] John W. ROBBINS[1]

[1]SGT Inc., Cryospheric Sciences Branch, NASA Goddard Space Flight Center, Code 614.1, Greenbelt, MD 20771, USA
E-mail: donghui.yi@nasa.gov
[2]Cryospheric Sciences Branch, NASA Goddard Space Flight Center, Code 614.1, Greenbelt, MD 20771, USA

**ABSTRACT. Sea-ice freeboard heights for 17 ICESat campaign periods from 2003 to 2009 are derived from ICESat data. Freeboard is combined with snow depth from Advanced Microwave Scanning Radiometer for Earth Observing System (AMSR-E) data and nominal densities of snow, water and sea ice, to estimate sea-ice thickness. Sea-ice freeboard and thickness distributions show clear seasonal variations that reflect the yearly cycle of growth and decay of the Weddell Sea (Antarctica) pack ice. During October–November, sea ice grows to its seasonal maximum both in area and thickness; the mean freeboards are 0.33–0.41 m and the mean thicknesses are 2.10–2.59 m. During February–March, thinner sea ice melts away and the sea-ice pack is mainly distributed in the west Weddell Sea; the mean freeboards are 0.35–0.46 m and the mean thicknesses are 1.48–1.94 m. During May–June, the mean freeboards and thicknesses are 0.26–0.29 m and 1.32–1.37 m, respectively. The 6 year trends in sea-ice extent and volume are $(0.023 \pm 0.051) \times 10^6$ km$^2$ a$^{-1}$ (0.45% a$^{-1}$) and $(0.007 \pm 0.092) \times 10^3$ km$^3$ a$^{-1}$ (0.08% a$^{-1}$); however, the large standard deviations indicate that these positive trends are not statistically significant.**

## 1. INTRODUCTION

Antarctic sea ice is dominated by seasonal sea ice. Sea-ice extent in summer is only about 15% of that in winter (Comiso and Nishio, 2008). To understand the sea-ice mass balance, the seasonal variation of both sea-ice extent (area with concentration greater than, e.g., 15%) and thickness must be measured. Currently, sea-ice extent and concentration are monitored daily by passive-microwave satellite remote sensing (Gloersen and others, 1992; Markus and Cavalieri, 1998; Comiso and others, 2003). However, there are no corresponding basin-scale thickness observations.

In the past few decades, considerable efforts have been made to measure sea-ice freeboard and thickness in the Southern Ocean. Ship-based measurements (Ackley, 1979; Wadhams and others, 1987; Lange and Eicken, 1991; Worby and others, 2008b), airborne remote sensing (Leuschen and others, 2008; Lieser and others, in press) and upward-looking sonar (ULS) (Strass and Fahrbach, 1998; Drinkwater and others, 2001; Harms and others, 2001; Worby and others, 2001; Renner and Lytle, 2007) have covered various locations and different seasons in the Southern Ocean. These measurements are sparsely located and/or sparsely distributed in time, and the sampled areas were mostly at the margins of the Antarctic sea-ice pack that is accessible by ships. Therefore, available sea-ice freeboard and thickness estimates tend to be from the thin end of the thickness distribution.

The most comprehensive dataset of Antarctic sea-ice thickness to date is from the Antarctic Sea Ice Processes and Climate (ASPeCt) project summarized by Worby and others (2008b). This is a compilation of 21 710 individual ship-based observations from 81 voyages and 1663 aircraft-based observations. The observations cover two and a half decades from 1981 to 2005. However, significant regional and seasonal gaps exist. The limitations of surface-based observations demonstrate that only satellite observations can provide the necessary spatial and temporal observation coverage to systematically study the sea ice in the Southern Ocean. Recent radar altimetry data have been used to study the sea-ice surface elevations (Giles and others, 2008), but the large footprint and the penetration effect of the radar altimetry data make it difficult to retrieve sea-ice freeboard or thickness in the Southern Ocean. Hopefully, the more sophisticated instrument design and retracking method of CryoSat2 will improve the performance of the radar altimeter in the Southern Ocean.

NASA's Ice, Cloud and land Elevation Satellite (ICESat; 2003–09) has been used to measure sea-ice freeboard and thickness in both the Arctic (Kwok and others, 2004, 2006, 2007, 2009; Kwok and Cunningham, 2008; Farrell and others, 2009; Spreen and others, 2009; Yi and Zwally, http://earth.esa.int/cryosat2005/participants/69/pres_yi.pdf) and the Southern Ocean (Zwally and others, 2008; Lieser and others, in press; Xie and others, in press; Yi and Zwally, http://earth.esa.int/cryosat2005/participants/69/pres_yi.pdf). Zwally and others (2008) demonstrated that ICESat surface elevation profile can be used to retrieve sea-ice freeboard and can be combined with Advanced Microwave Scanning Radiometer for Earth Observing System (AMSR-E) snow depth to estimate thickness in the Weddell Sea, Antarctica. We apply a technique similar to that of Zwally and others (2008) to derive sea-ice freeboard from ICESat elevation profiles and estimate sea-ice thickness over the Weddell Sea for 17 observation periods extending from February 2003 to April 2009. For the first time, the seasonal and interannual variations of basin-scale sea-ice freeboard and thickness in the Southern Ocean are observed during the 6 year ICESat observation period.

https://doi.org/10.3189/172756411795931480 Published online by Cambridge University Press

**Table 1.** ICESat campaign period, operating time, Antarctic season when measurements were made, repeat orbit period, and month–year label for each campaign. Seasons are: summer (JFM), fall (AMJ), winter (JAS) and spring (OND)

| Campaign period | Start date | End date | Operating time days | Antarctic season | Orbit days | MMYYYY |
|---|---|---|---|---|---|---|
| Laser 1 | 20 Feb 2003 | 29 Mar 2003 | 38 | Summer | 8 | FM2003 |
| Laser 2a | 25 Sep 2003 | 19 Nov 2003 | 10/47 | Early spring | 8/91 | ON2003 |
| Laser 2b | 17 Feb 2004 | 21 Mar 2004 | 34 | Summer | 91 | FM2004 |
| Laser 2c | 18 May 2004 | 21 Jun 2004 | 35 | Fall | 91 | MJ2004 |
| Laser 3a | 3 Oct 2004 | 8 Nov 2004 | 37 | Early spring | 91 | ON2004 |
| Laser 3b | 17 Feb 2005 | 24 Mar 2005 | 36 | Summer | 91 | FM2005 |
| Laser 3c | 20 May 2005 | 23 Jun 2005 | 35 | Fall | 91 | MJ2005 |
| Laser 3d | 21 Oct 2005 | 24 Nov 2005 | 35 | Early spring | 91 | ON 2005 |
| Laser 3e | 22 Feb 2006 | 28 Mar 2006 | 35 | Summer | 91 | FM2006 |
| Laser 3f | 24 May 2006 | 26 Jun 2006 | 35 | Fall | 91 | MJ2006 |
| Laser 3g | 25 Oct 2006 | 27 Nov 2006 | 34 | Early spring | 91 | ON2006 |
| Laser 3h | 12 Mar 2007 | 14 Apr 2007 | 34 | Summer | 91 | MA2007 |
| Laser 3i | 2 Oct 2007 | 5 Nov 2007 | 35 | Early spring | 91 | ON2007 |
| Laser 3j | 17 Feb 2008 | 21 Mar 2008 | 34 | Summer | 91 | FM2008 |
| Laser 3k | 4 Oct 2008 | 19 Oct 2008 | 16 | Early spring | 91 | O2008 |
| Laser 2d | 25 Nov 2008 | 17 Dec 2008 | 23 | Spring | 91 | ND2008 |
| Laser 2e | 9 Mar 2009 | 11 Apr 2009 | 34 | Summer | 91 | MA2009 |
| Laser 2f | 30 Sep 2009 | 11 Oct 2009 | 12 | Early spring | 91 | SO2009 |

## 2. DATA

In January 2003, NASA launched ICESat with a precision laser altimeter system for measuring surface elevations (Zwally and others, 2002a; Schutz and others, 2005). The precision of ICESat measurements of mean surface elevations of flat surfaces is 2 cm over 70 m laser footprints spaced at 172 m (Kwok and others, 2004; Yi and Zwally, http://earth.esa.int/cryosat2005/participants/69/pres_yi.pdf), providing a powerful new tool for studying sea-ice freeboard and thickness. The ICESat orbit extends to polar latitudes of 86°, and provides coverage of all sea ice in the Southern Ocean surrounding Antarctica and most of the sea ice in the Arctic Ocean. Due to lifetime limitations of ICESat's three lasers, ICESat operated periodically from 2003 to 2009.

The operational periods are of 34–38 days, except for four periods when special events happened. (1) The September–November 2003 period has 57 days; during that period, ICESat operation changed from an 8 day calibration/validation orbit to a 91 day operation orbit. (2) In October 2008, ICESat laser 3 failed, limiting that operation period to 16 days; subsequently, (3) an extra 23 days of laser 2 operation was added to complete the ground track lost in October 2008 with an additional few days of orbit overlap. (4) The last campaign period lasted for 12 days; ICESat laser 2 failed on 11 October 2009, prematurely ending this campaign. Data from this short and final period are not used in this study. Table 1 lists the campaign periods, operating times, Antarctic seasons and repeat orbits of ICESat observations.

ICESat data products GLA05 and GLA06 from February 2003 to April 2009 are used in this study. We use data release 428 for data products from laser 1 to laser 3j, release 429 for laser 3k, release 530 for laser 2d, and release 531 for laser 2e. Similar to Zwally and others (2008), the following conditions were adopted to filter out data contaminated by clouds, saturation and land/islands.

1. Gain limit: an upper limit of detector gain is applied to filter out stronger atmospheric attenuated waveforms. For the high-energy campaign periods (laser 1, 2a, 2b, 3a and 3b), the gain limit is set at 50 counts. For the low-energy campaign periods (laser 2d and 2e), no gain limit is applied. For the mid-energy campaigns (laser 2c, 3j, 3k, and laser 3c, 3d, 3e, 3f, 3g, 3h, 3i) the gain limits are set at 120 and 80 counts respectively. Gain limit has to be empirically adjusted, since lower laser energy penetrates less cloud and gain associated with atmospheric forward-scattered waveforms increases while laser energy decreases.

2. Pulse-broadening limit: we define a pulse-broadening parameter,

$$S = \frac{c}{2}\sqrt{\sigma_R^2 - \sigma_T^2}, \quad (1)$$

where $\sigma_R$ is the echo waveform $1\sigma$ pulse width, $\sigma_T$ is the transmitted waveform $1\sigma$ pulse width, and $c$ is the speed of light. $S$ measures the broadening of the transmitted pulse associated with surface topography and the undesirable effects of saturation and atmospheric forward scattering. Heavily saturated waveforms and forward-scattering waveforms have broadened pulse widths, so data with $S > 0.8$ m are discarded.

3. Reflectivity limit: heavily saturated waveforms also tend to have very high apparent reflectivity, and forward-scattering waveforms tend to have low reflectivity, so data with reflectivity smaller than 0.05 or larger than 0.9 are discarded.

Since ICESat elevation data do not distinguish surface types such as water, sea ice or land, AMSR-E ice concentration is used to separate sea ice from land and water. In this study, only areas with ice concentration more than 60% are considered.

The snow-depth and ice-concentration (NASA Team) data used in this study are from AMSR-E (Markus and Cavalieri, 1998; Comiso and others, 2003). For the study area, we used data in the Weddell Sea between the Antarctic Peninsula and 0° longitude.

https://doi.org/10.3189/172756411795931480 Published online by Cambridge University Press

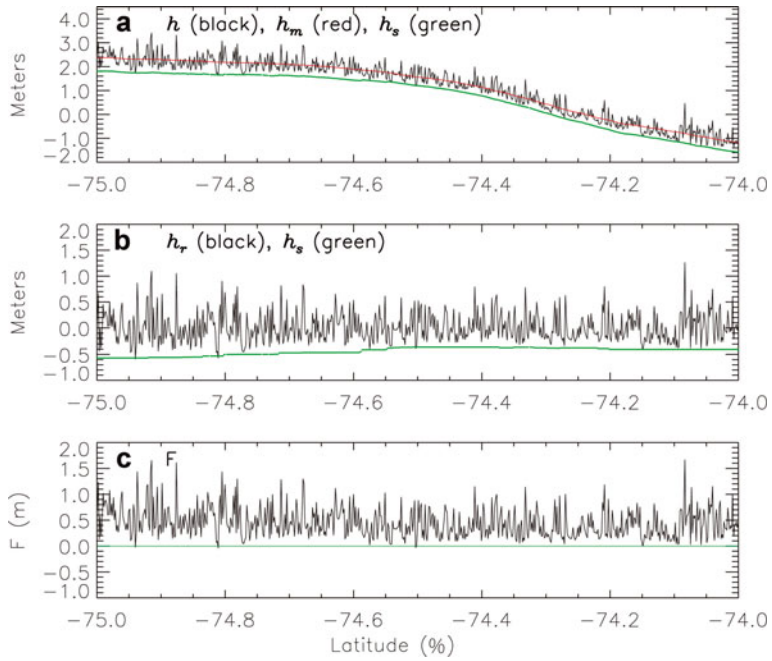


**Fig. 1.** An example of $h_m$, $h_s$, $h_r$ and $F$ calculation. The profile is from October to November 2003. (a) Elevation, $h$, is referenced to the Earth Gravitational Model 1996 (EGM96) geoid. $h_m$ is the 20 km running mean of $h$. (b) Relative elevation, $h_r$ ($=h-h_m$). Ocean level, $h_s$, is determined by averaging the lowest 2% of the $h_r$ values within ±25 km of a point. (c) Freeboard height, $F=h_r-h_s$.

## 3. METHOD

Details of the technique used to derive sea-ice freeboard from ICESat elevation profiles are provided by Zwally and others (2008). In brief, the technique of deriving freeboards uses segments of open water and thin ice detected by the laser altimeter to determine the height of the along-track ocean surface, which is then used as the ocean reference level for the freeboard heights of the snow-covered sea ice. Freeboard is defined here as the total height of the snow cover and sea ice above the ocean (whereas it is sometimes used to refer to only the sea-ice portion, leading to the possibility of so-called negative freeboards).

After establishing the ocean reference level for each ICESat along-track elevation measurement, the freeboard height is determined relative to this reference level. The ICESat detection of open-water and thin-ice areas was demonstrated by Kwok and others (2006) and Zwally and others (2008) in comparison with available Envisat synthetic aperture radar (SAR) images that show leads and polynyas with thin ice and open water. Estimation of sea-ice thickness from the freeboards requires additional information and a number of assumptions about the densities and thicknesses of the snow cover and the sea ice. The parameters required to retrieve sea-ice thickness here are similar to estimations of sea-ice thickness from radar altimetry (Laxon and others, 2003) and submarine sonar measurement of sea-ice drafts (Rothrock and others, 1999).

### 3.1. Elevation and relative elevation

The ICESat-measured surface elevation, $H_{ie}$, is referenced to an Earth ellipsoid, as used by TOPEX/Poseidon and Jason-1. ICESat surface elevations have instrument corrections, dry and wet troposphere corrections and tidal corrections applied. We also applied saturation correction and inverse barometer correction (Zwally and others, 2008). In the following analysis, we define the elevation, $h$, above the geoid as

$$h = H_{ie} + \Delta H_{ib} + H_{sat} - h_g, \quad (2)$$

where $\Delta H_{sat}$ is the saturation correction and $h_g$ is the geoid height. Note that the influence of $\Delta H_{ib}$, $\Delta H_{sat}$ and $h_g$ are removed from $H_{ie}$, but other factors such as dynamic topography and the residuals in the static geoid still affect $h$.

Due to the limited accuracy of the geoids and ocean tide models, and limited knowledge of the dynamic topography, sea-ice surface elevation referenced to a geoid cannot be regarded as sea-ice freeboard. Computing sea-ice freeboard requires the elevation difference between the top of the snow surface on the sea ice and local ocean levels. If the elevation difference is known, even if the absolute elevations are biased, the sea-ice freeboard can still be determined. By determining local ocean level and using only the relative elevation, effects of the longer-wavelength (>20 km) factors, such as geoid error, long-wavelength laser pointing error and tidal error (which affect the absolute elevation), are removed from the freeboard calculation.

### 3.2. Freeboard calculation

Figure 1 shows an example of computed freeboard from an elevation profile over the Weddell Sea from October to November 2003. In Figure 1a, elevation, $h$, is referenced to the geoid. To remove the long-wavelength geoid error, tidal error and dynamic ocean topography, we compute a 20 km running mean, $h_m$, of $h$, which is then used as a reference level (Fig. 1b) in the computation of relative elevations, $h_r$ ($h-h_m$). In this study, leads (open water and thin ice) in the sea ice are considered to be at ocean level. Ocean level, $h_s$, at any given point is determined by averaging the lowest 2% of the $h_r$ values within ±25 km of that point.

Freeboard height, $F$, at a given point is defined as $F=h_r-h_s$. To have a valid $F$ at a point, there must be enough valid elevation measurements available within

https://doi.org/10.3189/172756411795931480 Published online by Cambridge University Press

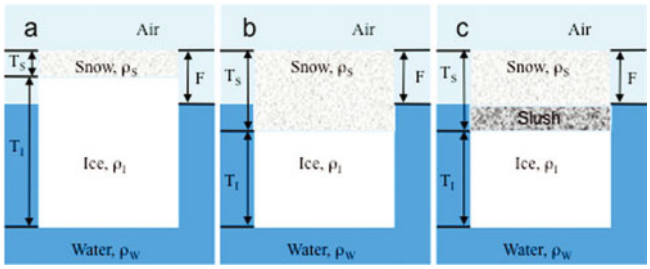


**Fig. 2.** Three typical cases of sea ice in the Southern Ocean. (a) The most common state, with a layer of snow on top of ice, and the snow/ice interface above sea level. (b) Over the Southern Ocean, the snow/ice boundary frequently fell below sea level, mainly due to the accumulation of snow on the snow/air interface. The sea ice can stay in this state for an extended period; eventually sea water will penetrate the sea ice from below or flow from the sides to form slush and then refreeze as shown in (c).

±25 km of that point. In this study, a point is discarded if <50% of the total 300 points are available. After freeboard at each point along an elevation profile is calculated, freeboards from ground tracks of each campaign period are gridded to 25 km × 25 km gridcells. The 2% value was selected empirically. It provides enough points in calculating mean sea level to reduce measurement noise, and minimizes the influence of thin ice in the calculation. In cases when open water is <2% within the 50 km range, $h_s$ will measure the height of thin ice, thus underestimating freeboard. Figure 1c shows freeboard height $F = h_r - h_s$.

### 3.3. Thickness calculation

There are three typical states of sea ice in the Southern Ocean (Fig. 2). Figure 2a is the most common state, with a layer of snow on top of ice, and the snow/ice interface above sea level. This state is described by Giles and others (2008) and Zwally and others (2008) over the Southern Ocean and by Kwok and others (2009) over the Arctic. Over the Southern Ocean, however, the snow/ice boundary frequently fell below sea level (Lange and others, 1990; Lytle and Ackley, 1996) (Fig. 2b), mainly due to the accumulation of snow. The sea ice can stay in this state for an extended period; eventually sea water will penetrate the sea ice or flow from the sides to form slush and then refreeze in 2–3 weeks (Lytle and Ackley, 1996) (Fig. 2c). For the state in Figure 2a, sea-ice thickness, $T_I$, is a function of freeboard height, $F$, snow depth, $T_S$, snow density, $\rho_S$, water density, $\rho_W$, and sea-ice density, $\rho_I$. According to Archimedes' buoyancy principle,

$$T_I = \frac{\rho_W}{\rho_W - \rho_I} F - \frac{\rho_W - \rho_S}{\rho_W - \rho_I} T_S. \quad (3)$$

In this study, constant densities of $\rho_S = 300\,\mathrm{kg\,m^{-3}}$, $\rho_W = 1023.9\,\mathrm{kg\,m^{-3}}$ and $\rho_I = 915.1\,\mathrm{kg\,m^{-3}}$ (Laxon and others, 2003) are used to calculate sea-ice thickness from the freeboard. $T_I$ can then be expressed as

$$T_I = 9.411F - 6.653T_S. \quad (4)$$

For the state in Figure 2c, $F = T_s$ and, assuming $\rho_{slush} = \rho_I$, Equation (3) becomes

$$T_I = \frac{\rho_S}{\rho_W - \rho_I} F. \quad (5)$$

$T_I$ can then be expressed as

$$T_I = 2.757F. \quad (6)$$

We recognize that ice thickness is sensitive to the local and regional variability of snow and ice densities. Since we have no detailed information about the errors in local densities, the error in $T_I$ is not calculated. In this study, the freeboard is always measured from snow/air or ice/air surface to sea level, hence it is always positive. If the snow depth is larger than freeboard, snow depth is set equal to the freeboard, as in Zwally and others (2008). This treatment is equivalent to assuming the state in Figure 2b will turn into the state in Figure 2c and then the slush freezes. This will introduce an unknown error in thickness before the state in Figure 2b turns into the state in Figure 2c.

## 4. RESULTS

Sea-ice freeboard heights for 17 ICESat campaign periods from March 2003 to April 2009 in the Weddell Sea were derived from ICESat laser altimeter measurements. Thickness is estimated by combining ICESat freeboard, AMSR-E snow depth and nominal densities of snow, water and sea ice. Sea-ice freeboard and thickness distributions show clear seasonal variations that reflect the yearly cycle of the growth and decay of the Weddell Sea pack ice.

### 4.1. Freeboard

Freeboard maps and distributions are shown in Figure 3. The seasonal sea-ice area variation is clearly presented here for every year of the observations from 2003 to 2009. The area minimum is in the February–March (summer) periods. For the five February–March periods, the mean freeboards are 0.35–0.46 m. Mean freeboards for the two March–April periods are 0.34 and 0.43 m. Large portions of thin ice formed in the May–June periods (fall). For the three fall periods, the mean freeboards vary from 0.26 to 0.29 m. Maximum areas are in the October–November periods (early spring); for the six early-spring periods, mean freeboards are 0.33–0.41 m. The mean freeboard and the standard deviation of the mean freeboard are listed in Table 2.

In general, the freeboard increases from east to west in the Weddell Sea for all seasons, with the maximum values along the east coast of the Antarctic Peninsula. The C-shaped patterns associated with the Weddell Gyre are notable in the fall and spring. While sea-ice area reaches minimums in February–March, the mean freeboards are comparable to the values of early spring, but remain larger than the fall values. This is due to the summer survival of thick sea ice and the melt of thin sea ice over the season. As might be expected, mean freeboards are larger in March–April than in May–June. The November–December period in 2008 shows the spring melting; the area is much smaller than in the October–November periods.

### 4.2. Thickness

Figure 4 shows the sea-ice thickness computed via Equations (4) and (6), based on ICESat freeboard and AMSR-E snow depth. Equation (4) is used for most of the gridcells. For areas with $T_S > F$, we assume the areas will be flooded and then refreeze, and set snow depth, $T_S$, equal to freeboard, $F$, in our calculation. This assumption will introduce errors in thickness before the sea ice is flooded and before the slush refreezes. However, for most of the $T_S > F$ case, the sea ice

https://doi.org/10.3189/172756411795931480 Published online by Cambridge University Press

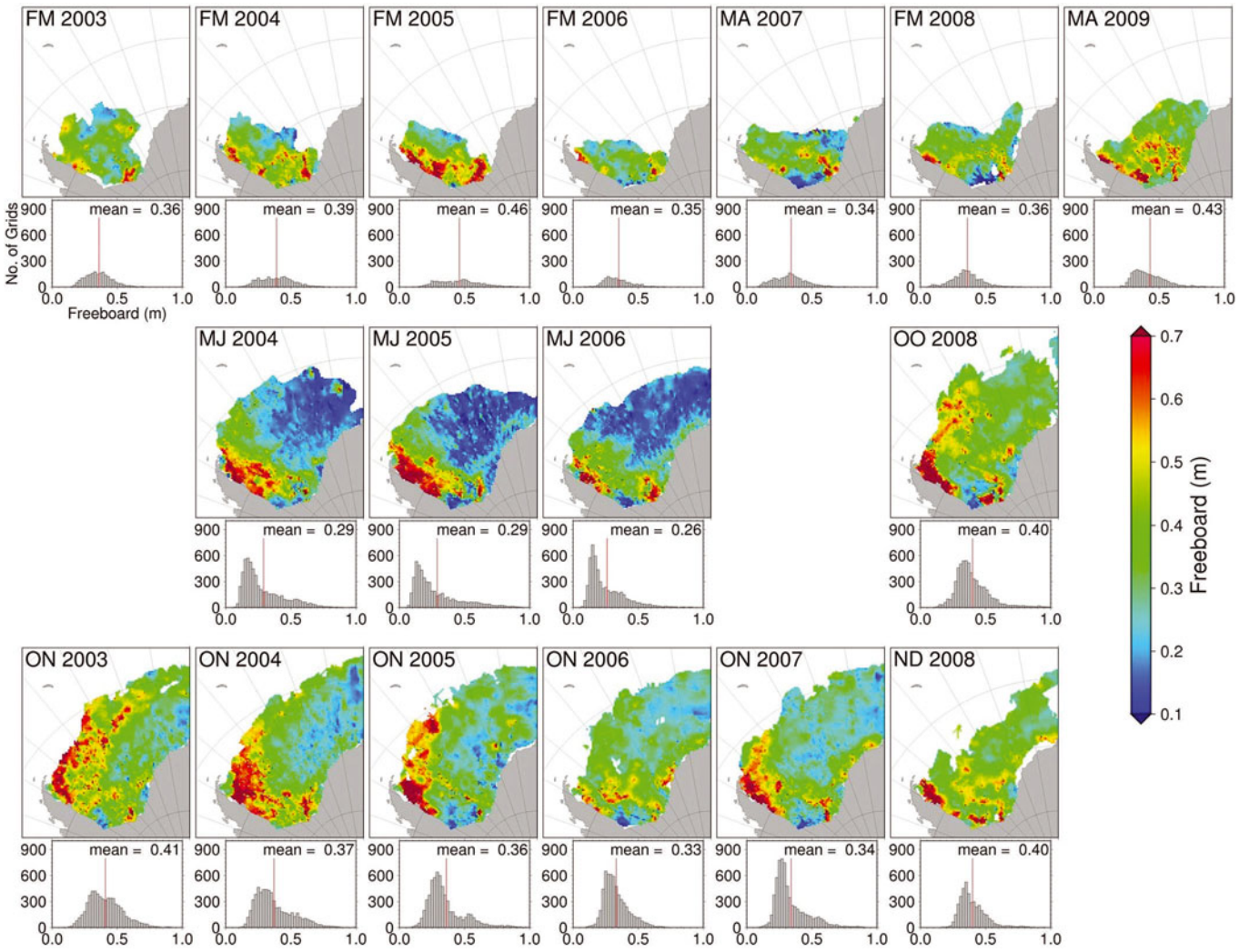


**Fig. 3.** Sea-ice freeboard for 17 campaign periods. The red lines are at the mean freeboards of the histograms. During the February–March periods, values of the modes and means are comparable and the histogram shapes are close to normal distribution. During the May–June periods, the histograms are heavily positively skewed, and the modes are much smaller than the means, reflecting the rapid growth of the newly formed thin ice. During the October–November periods, the histograms are less skewed, the means are larger than for the May–June period and the modes are closer to the means, reflecting the growth in thickness of the previously formed thin ice. Due to surface freeboard changes during a campaign period and multiple satellite measurement occurring at different times, some stripe-type features are visible, especially for the May–June periods, reflecting rapid growth in the fall season.

will be flooded and the slush will refreeze in 2–3 weeks (Lange and others, 1990; Lytle and Ackley, 1996). The spatial distribution patterns in the thickness maps are similar to those in the freeboard maps. For the five February–March periods, the mean thicknesses, $T_I$, range from 1.48 to 1.94 m. For the three fall periods, they range from 1.32 to 1.37 m. For the six October–November periods, they range from 2.10 to 2.59 m. The mean thickness and the standard deviation of the mean thickness are listed in Table 2.

In general, the thickness increases from the eastern to the western Weddell Sea for all seasons, with the maximum values along the east coast of the Antarctic Peninsula. A C-shaped pattern of the Weddell Gyre is also notable in the fall and spring seasons. The thickness distribution in October–November shows the largest annual variations: there is thick ice distributed along the northwest side of the Weddell Sea in 2003, 2004, 2005 and 2007, but not much thick ice in the area in 2006 and 2008; in 2006, there is more thick ice distributed in the central west Weddell Sea than in the other October–November periods.

An underestimate of snow depth will produce a positive bias of sea-ice thickness and vice versa. Worby and others (2008a) found that AMSR-E snow depth over the Antarctic can underestimate snow depth by a factor of 2.3 for rough sea-ice regions; if proven, this would make the calculated thickness appear higher in this study. Xie and others (in press) compared ICESat freeboard and thickness with their in situ cruise measurement in the Bellingshausen–Amundsen Seas under ICESat ground track during October 2007. They concluded that the ICESat freeboard ($0.42 \pm 0.24$ m) and thickness ($1.38 \pm 0.70$ m) in the studied area agree with their in situ measurements ($0.36 \pm 0.28$ m and $1.26 \pm 0.94$ m, respectively) reasonably well. Lieser and others (in press) compared an airborne laser altimetry and ICESat freeboard in East Antarctica, also during October 2007. The freeboard from the airborne laser was $0.59 \pm 0.52$ m and from ICESat was $0.41 \pm 1.26$ m. The large differences may reflect the high drift rate of the ice (19 km d$^{-1}$), which may produce large fluctuations in mean freeboard in the region. However, due to different sea-ice characteristics, results from the

https://doi.org/10.3189/172756411795931480 Published online by Cambridge University Press

**Table 2.** Campaign periods, mean freeboard, standard deviation of mean freeboard, mean thickness ($T$), standard deviation of mean thickness, and flooding-related parameters

| Campaign period | Mean $F$ | SD of mean $F$ | $T$ | SD of $T$ | $T_S > F$ | Mean $F - T_S$ | $T_F/T$ | MMYYYY |
|---|---|---|---|---|---|---|---|---|
| | m | m | m | m | % | m | % | |
| Laser 1 | 0.36 | 0.002 | 1.5 | 0.02 | 42.8 | 0.02 | 66 | FM2003 |
| Laser 2a | 0.41 | 0.002 | 2.59 | 0.01 | 0.1 | 0.22 | 44 | ON2003 |
| Laser 2b | 0.39 | 0.003 | 1.55 | 0.02 | 39.1 | 0.02 | 70 | FM2004 |
| Laser 2c | 0.29 | 0.002 | 1.32 | 0.01 | 19.7 | 0.06 | 61 | MJ2004 |
| Laser 3a | 0.37 | 0.002 | 2.19 | 0.02 | 8.5 | 0.16 | 47 | ON2004 |
| Laser 3b | 0.46 | 0.004 | 1.94 | 0.04 | 40.3 | 0.05 | 65 | FM2005 |
| Laser 3c | 0.29 | 0.003 | 1.37 | 0.02 | 13.8 | 0.08 | 58 | MJ2005 |
| Laser 3d | 0.36 | 0.002 | 2.25 | 0.01 | 0.2 | 0.19 | 44 | ON 2005 |
| Laser 3e | 0.35 | 0.003 | 1.71 | 0.03 | 20.2 | 0.08 | 56 | FM2006 |
| Laser 3f | 0.26 | 0.002 | 1.32 | 0.01 | 11.4 | 0.06 | 55 | MJ2006 |
| Laser 3g | 0.33 | 0.001 | 2.12 | 0.01 | 4.2 | 0.17 | 43 | ON2006 |
| Laser 3h | 0.34 | 0.003 | 1.58 | 0.02 | 20.1 | 0.08 | 59 | MA2007 |
| Laser 3i | 0.34 | 0.002 | 2.19 | 0.01 | 0.7 | 0.19 | 43 | ON2007 |
| Laser 3j | 0.36 | 0.003 | 1.48 | 0.02 | 29.4 | 0.04 | 67 | FM2008 |
| Laser 3k | 0.40 | 0.002 | 2.10 | 0.02 | 2.9 | 0.14 | 52 | O2008 |
| Laser 2d | 0.40 | 0.002 | 2.86 | 0.02 | 0.3 | 0.26 | 38 | ND2008 |
| Laser 2e | 0.43 | 0.003 | 2.16 | 0.02 | 19.6 | 0.12 | 55 | MA2009 |

Bellingshausen–Amundsen Seas and East Antarctica may not be applicable to the Weddell Sea.

### 4.3. Flooding

In the Weddell Sea, the snow/ice boundary frequently falls below sea level and becomes flooded ($T_S > F$). Lytle and Ackley (1996) estimated that ~50% of the area was flooded in February–March in the west Weddell Sea during their 1992 field season. Table 2 lists the percentage of gridcells with $T_S > F$ and the mean of $F - T_S$. In the five February–March periods, the number of $T_S > F$ cells ranges from 20.2% to 42.8%. The highest percentage in the three observed seasons, 42.8%, is comparable with Lytle and Ackley's estimate. In the six October–November periods, the number of $T_S > F$ cells ranges from 0.1% to 8.5%, with three periods less than 1%. The three May–June periods have modest flooding percentages, 11.4–19.7%, smaller than the February–March ranges and larger than the October–November ranges. The mean $F - T_S$ values in Table 2 show small values range from 0.02 to 0.08 m in the February–March periods, indicating the snow depth, $T_S$, and freeboard, $F$, are very close when a large percentage of cells are flooded. On the other hand, when the percentage of $T_S > F$ are low in the October–November periods, the mean $F - T_S$ values are high, ranging from 0.14 to 0.22 m, and very few flooding events occur.

We evaluate the possible snow-depth error introduced by its uncertainty and flooding by assuming snow depth equals ICESat-measured freeboard; this is equivalent to using Figure 2c and Equation (6) to represent all situations. Although this is an oversimplification for most of the time, it provides an estimate of sea-ice thickness independent of any snow-depth data input.

Let $T_F$ represent the mean thickness calculated from Equation (6) only and $T$ represent the mean $T_I$ for each period. The $T_F/T$ ratios for each campaign period are listed in Table 2. For the five February–March periods, the ratios are 56–70%. For the six October–November periods, they are 43–52%. The higher $T_F/T$ values for the February–March periods reflect the smaller differences of $F$ and $T_S$ listed in Table 2, and the lower $T_F/T$ values for the October–November periods reflect the larger $F$ and $T_S$ differences.

### 4.4. Geoid and dynamic ocean topography

After removing the geoid and inverted barometer effects, the elevation signal is still dominated by the unresolved geoid residuals and the dynamic ocean topography. Here we define the difference between ICESat-measured sea level ($h_s$, referenced to $h_m$) and the Earth Gravitational Model 1996 (EGM96) geoid ($h_g$) as $h_d = h_m + h_s$. In Figure 5 the consistent pattern of different campaign periods indicates that a major portion of $h_d$ is due to time-invariant factors, most likely uncertainties in the geoid and unmodeled dynamic ocean topography. The possible contributors to the time-variant portion of $h_d$ are ICESat laser-pointing errors, tidal errors and unmodeled dynamic ocean topography. We have calculated the mean $h_d$ grid of all 17 campaign periods in the sea-ice covered regions. The average $h_d$ grid can be treated as a new mean sea level of the studied region. This result demonstrates that ICESat data could be used to improve the geoid model in the Southern Ocean and mapping of dynamic ocean topography. Forsberg and Skourup (2005) used some early ICESat data and Gravity Recovery and Climate Experiment (GRACE) data to improve an Arctic geoid model.

## 5. DISCUSSION AND CONCLUSIONS

We have derived sea-ice freeboard over the Weddell Sea, using ICESat-measured surface elevation. Combining ICESat freeboard with AMSR-E passive microwave snow depth and nominal densities of snow, sea ice and water, we estimated sea-ice thickness. The freeboard and thickness maps in the Weddell Sea for 17 campaign periods show seasonal and interannual variations.

We calculated sea-ice extent and volume for grids with AMSR-E ice concentration higher than 60% for each campaign period over the Weddell Sea. To derive the trends over the 6 years, a sinusoidal function with a yearly cycle and a linear trend is used to fit the sea-ice extent and

https://doi.org/10.3189/172756411795931480 Published online by Cambridge University Press

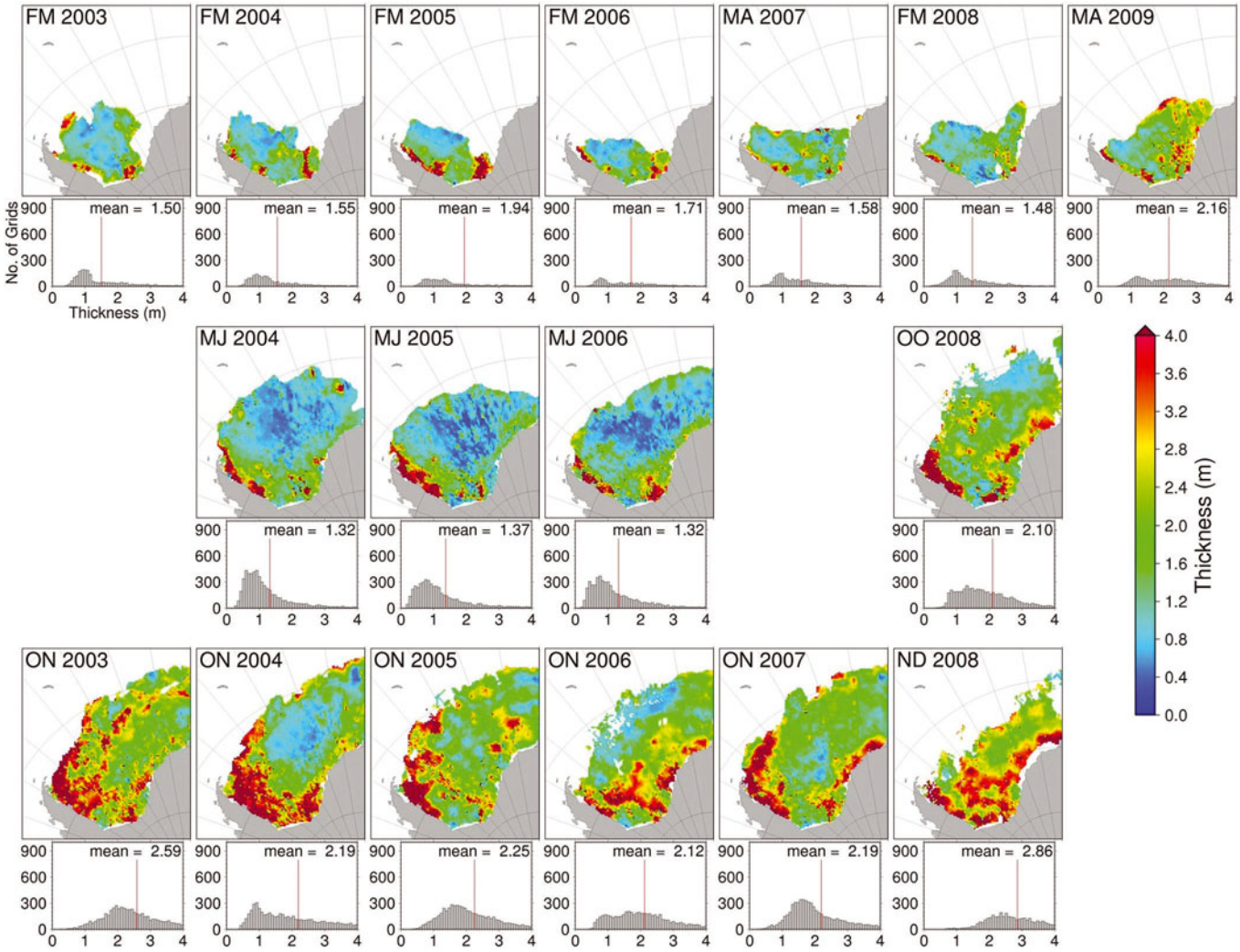


**Fig. 4.** Sea-ice thickness for 17 campaign periods. The red lines are at the mean thickness of the histograms. During February–March periods, unlike for the freeboard, the histograms are not close to normal distribution, the small amount of thick ice increased the means and the modes are lower, ~1 m. During the May–June periods, the newly formed thin ice reduces both means and modes compared to the February–March periods. During the October–November periods, both modes and means continue to grow compared to the May–June period, reflecting the growth in thickness of the previously formed thin ice.

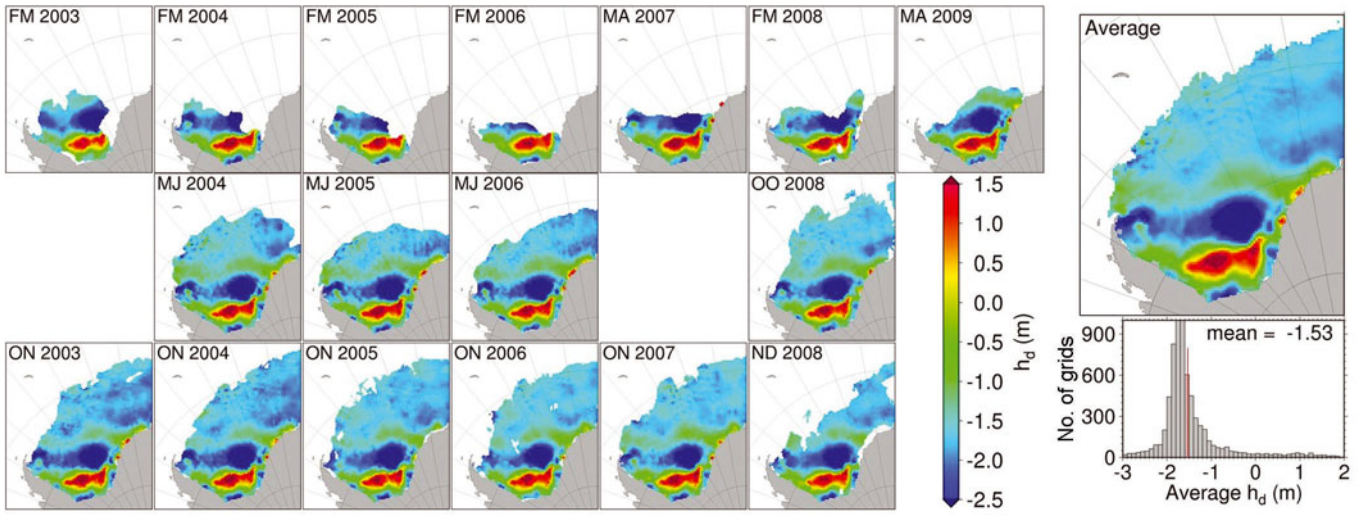


**Fig. 5.** Mean sea level above EGM96 geoid ($h_d$) for 17 periods and their average.

https://doi.org/10.3189/172756411795931480 Published online by Cambridge University Press

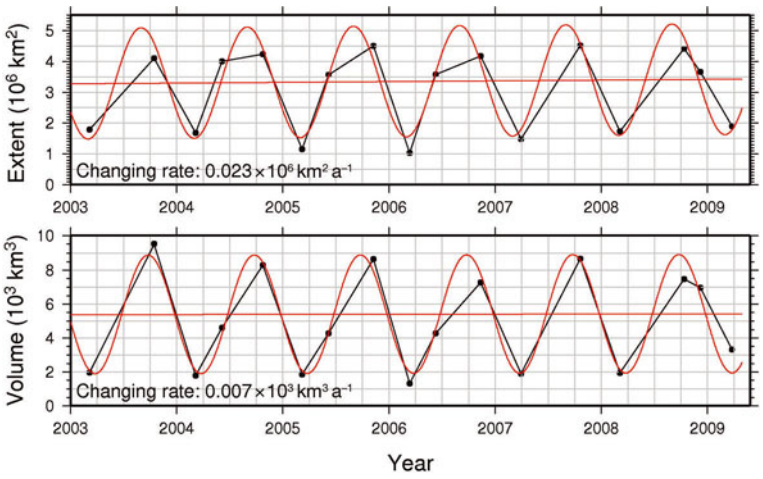


**Fig. 6.** Weddell Sea ice extent and volume from 2003 to 2009. A sinusoidal function with a yearly cycle and a linear trend, $y = y_0 + at + A\cos(\omega t + \varphi)$, is used to fit both sea-ice extent and volume time series. During the 6 year period, the changing rate for extent is $(0.023 \pm 0.051) \times 10^6$ km$^2$ a$^{-1}$; the changing rate for volume is $(0.007 \pm 0.092) \times 10^3$ km$^3$ a$^{-1}$. The peak-to-peak amplitudes of the seasonal cycle are $3.6 \times 10^6$ km$^2$ in extent and $7.0 \times 10^3$ km$^3$ in volume.

volume time series (Fig. 6). Although the observations are not continuous and not at exactly the same time of year, the multi-function fitting matches the observations well. The 6 year trends in sea-ice extent and volume are $(0.023 \pm 0.051) \times 10^6$ km$^2$ a$^{-1}$ (0.45% a$^{-1}$) and $(0.007 \pm 0.092) \times 10^3$ km$^3$ a$^{-1}$ (0.08% a$^{-1}$), indicating small increases with time. However, the large standard deviations relative to the calculated trends indicate that these positive trends are not statistically significant. Future satellite laser altimeter missions (e.g. ICESat-2) will permit continued monitoring of freeboard, producing monthly average maps, and will refine observations of the seasonal cycles and long-term trends derived from ICESat for the 2003–09 period.

The peak-to-peak amplitudes of the seasonal cycle are $3.6 \times 10^6$ km$^2$ in extent and $7.0 \times 10^3$ km$^3$ in volume. The extent trend, 4.5% (10 a)$^{-1}$ is much larger than the 0.7% (10 a)$^{-1}$ found by Comiso and Nishio (2008) for a much longer period (1979–2006). However, the standard deviation of the extent trend is large, and shorter-period subsets (~6 years) of Zwally and others (2002b) and Comiso and Nishio (2008) showed both larger positive and negative trends.

ICESat-determined sea level can potentially be used to improve the geoid and dynamic ocean topography knowledge in the sea-ice covered regions. An improved geoid will help improve sea-level determination and therefore improve ICESat measured freeboard accuracy. A better geoid will also help resolve the gravity field and tectonic features of a region (McAdoo and others, 2008). We will compare ICESat-determined sea level to a new geoid model, EGM08 (N.K. Pavlis and others, http://www.massentransporte.de/fileadmin/kolloquium_muc/2008-10-08/Bosch/EGM2008.pdf), in future studies.

Uncertainties in freeboard, snow depth, and densities of snow, water and ice introduce uncertainties in sea-ice thickness estimates. The precision of the AMSR-E snow depth is 5 cm (Comiso and others, 2003), based on Equation (4); this will lead to an uncertainty of ~33 cm in ice thickness. A similar study by Kwok and others (2007) on Arctic sea ice showed a freeboard uncertainty of ~5 cm. Based on Equation (4), this will lead to an uncertainty of ~47 cm in ice thickness. Discounting the error in the densities of snow, water and ice, the combined uncertainty due to ICESat freeboard and AMSR-E snow depth, based on Equation (4), is ~58 cm. We recognize that the uncertainty of the estimated sea-ice thickness is high. In future studies, better-calibrated snow depth and better-observed/-modeled densities of snow, water and sea ice are needed.

In situ measurements (e.g. sea-ice freeboard, thickness, snow depth and snow density) coincident with ICESat and AMSR-E measurements are necessary to further calibrate/validate the snow-depth, freeboard and thickness results. The analysis of Sea Ice Mass Balance in the Antarctic (SIMBA) cruise data (Xie and others, in press) and ASPeCt cruise data (Lieser and others, in press) show reasonable agreement between ICESat freeboard and thickness and in situ observations. Validation is difficult with point-wise measurements in the presence of ice drift, but the co-ordinated field experiments with both airborne and ground-based observations will make current and future satellite observations more credible as they can be more thoroughly compared with the in situ observations.

## ACKNOWLEDGEMENTS

This work is supported by NASA's funding of the ICESat Project Science. We thank A. Ivanoff, D. J. Cavalieri, T. Markus, and S. Fiegles for their help in providing the AMSR-E snow-depth and ice-concentration data. We thank both the Scientific Editor, S. Kern, and the two anonymous referees for their careful and helpful reviews.

## REFERENCES

Ackley, S.F. 1979. Mass-balance aspects of Weddell Sea pack ice. *J. Glaciol.*, **24**(90), 391–405.

Comiso, J.C. and F. Nishio. 2008. Trends in the sea ice cover using enhanced and compatible AMSR-E, SSM/I, and SMMR data. *J. Geophys. Res.*, **113**(C2), C02S07. (10.1029/2007JC004257.)

Comiso, J.C., D.J. Cavalieri and T. Markus. 2003. Sea ice concentration, ice temperature, and snow depth using AMSR-E data. *IEEE Trans. Geosci. Remote Sens.*, **41**(2), 243–252.

Drinkwater, M.R., X. Liu and S. Harms. 2001. Combined satellite- and ULS-derived sea-ice flux in the Weddell Sea, Antarctica. *Ann. Glaciol.*, **33**, 125–132.

https://doi.org/10.3189/172756411795931480 Published online by Cambridge University Press

Farrell, S.L., S.W. Laxon, D.C. McAdoo, D. Yi and H.J. Zwally. 2009. Five years of Arctic sea ice freeboard measurements from the Ice, Cloud and land Elevation Satellite. *J. Geophys. Res.,* **114**(C4), C04008. (10.1029/2008JC005074.)

Forsberg, R. and H. Skourup. 2005. Arctic Ocean gravity, geoid and sea-ice freeboard heights from ICESat and GRACE. *Geophys. Res. Lett.,* **32**(21), L21502. (10.1029/2005GL023711.)

Giles, K.A., S.W. Laxon and A.P. Worby. 2008. Antarctic sea ice elevation from satellite radar altimetry. *Geophys. Res. Lett.,* **35**(3), L03503. (10.1029/2007GL031572.)

Gloersen, P., W.J. Campbell, D.J. Cavalieri, J.C. Comiso, C.L. Parkinson and H.J. Zwally. 1992. *Arctic and Antarctic sea ice, 1978–1987: satellite passive-microwave observations and analysis.* Washington, DC, National Aeronautics and Space Administration. (NASA SP-511.)

Harms, S., E. Fahrbach and V.H. Strass. 2001. Sea ice transports in the Weddell Sea. *J. Geophys. Res.,* **106**(C5), 9057–9073.

Kwok, R. and G.F. Cunningham. 2008. ICESat over Arctic sea ice: estimation of snow depth and ice thickness. *J. Geophys. Res.,* **113**(C8), C08010. (10.1029/2008JC004753.)

Kwok, R., H.J. Zwally and D. Yi. 2004. ICESat observations of Arctic sea ice: a first look. *Geophys. Res. Lett.,* **31**(16), L16401. (10.1029/2004GL020309.)

Kwok, R., G.F. Cunningham, H.J. Zwally and D. Yi. 2006. ICESat over Arctic sea ice: interpretation of altimetric and reflectivity profiles. *J. Geophys. Res.,* **111**(C6), C06006. (10.1029/2005JC003175.)

Kwok, R., G.F. Cunningham, H.J. Zwally and D. Yi. 2007. Ice, Cloud, and land Elevation Satellite (ICESat) over Arctic sea ice: retrieval of freeboard. *J. Geophys. Res.,* **112**(C12), C12013. (10.1029/2006JC003978.)

Kwok, R., G.F. Cunningham, M. Wensnahan, I. Rigor, H.J. Zwally and D. Yi. 2009. Thinning and volume loss of the Arctic Ocean sea ice cover: 2003–2008. *J. Geophys. Res.,* **114**(C7), C07005. (10.1029/2009JC005312.)

Lange, M.A. and H. Eicken. 1991. The sea ice thickness distribution in the northwestern Weddell Sea. *J. Geophys. Res.,* **96**(C3), 4821–4837.

Lange, M.A., P. Schlosser, S.F. Ackley, P. Wadhams and G.S. Dieckmann. 1990. $^{18}O$ concentrations in sea ice of the Weddell Sea, Antarctica. *J. Glaciol.,* **36**(124), 315–323.

Laxon, S., N. Peacock and D. Smith. 2003. High interannual variability in sea ice thickness in the Arctic region. *Nature,* **425**(6961), 947–950.

Leuschen, C.J. *and 6 others*. 2008. Combination of laser and radar altimeter height measurements to estimate snow depth during the 2004 Antarctic AMSR-E Sea Ice field campaign. *J. Geophys. Res.,* **113**(C4), C04S90. (10.1029/2007JC004285.)

Lieser, J.L., R.A. Massom, A.P. Worby and D. Yi. In press. Antarctic sea ice freeboard from airborne laser altimetry and comparison with ICESat. *Deep-Sea Res. II.*

Lytle, V.I. and S.F. Ackley. 1996. Heat flux through sea ice in the western Weddell Sea: convective and conductive transfer processes. *J. Geophys. Res.,* **101**(C4), 8853–8868.

Markus, T. and D.J. Cavalieri. 1998. Snow depth distribution over sea ice in the Southern Ocean from satellite passive microwave data. *In* Jeffries, M.O., *ed. Antarctic sea ice: physical processes, interactions and variability.* Washington, DC, American Geophysical Union, 19–39. (Antarctic Research Series 74.)

McAdoo, D.C., S.L. Farrell, S.W. Laxon, H.J. Zwally, D. Yi and A.L. Ridout. 2008. Arctic Ocean gravity field derived from ICESat and ERS-2 altimetry: tectonic implications. *J. Geophys. Res.,* **113**(B5), B05408. (10.1029/2007JB005217.)

Renner, A.H.H. and V. Lytle. 2007. Sea-ice thickness in the Weddell Sea, Antarctica: a comparison of model and upward-looking sonar data. *Ann. Glaciol.,* **46**, 419–427.

Rothrock, D.A., Y. Yu and G.A. Maykut. 1999. Thinning of the Arctic sea-ice cover. *Geophys. Res. Lett.,* **26**(23), 3469–3472.

Schutz, B.E., H.J. Zwally, C.A. Shuman, D. Hancock and J.P. DiMarzio. 2005. Overview of the ICESat Mission. *Geophys. Res. Lett.,* **32**(21), L21S01. (10.1029/2005GL024009.)

Spreen, G., S. Kern, D. Stammer and E. Hansen. 2009. Fram Strait sea ice volume export estimated between 2003 and 2008 from satellite data. *Geophys. Res. Lett.,* **36**(19), L19502. (10.1029/2009GL039591.)

Strass, V.H. and E. Fahrbach. 1998. Temporal and regional variation of sea ice draft and coverage in the Weddell Sea obtained from upward looking sonars. *In* Jeffries, M.O., *ed. Antarctic sea ice: physical processes, interactions and variability.* Washington, DC, American Geophysical Union, 123–139. (Antarctic Research Series 74.)

Wadhams, P., M.A. Lange and S.F. Ackley. 1987. The ice thickness distribution across the Atlantic sector of the Antarctic Ocean in midwinter. *J. Geophys. Res.,* **92**(C13), 14,535–14,552.

Worby, A.P., G.M. Bush and I. Allison. 2001. Seasonal development of sea-ice thickness distribution in East Antarctica: measurements from upward-looking sonar data. *Ann. Glaciol.,* **33**, 177–180.

Worby, A.P., T. Markus, A.D. Steel, V.I. Lytle and R.A. Massom. 2008a. Evaluation of AMSR-E snow depth product over East Antarctic sea ice using in situ measurements and aerial photography. *J. Geophys. Res.,* **113**(C5), C05S94. (10.1029/2007JC004181.)

Worby, A.P., C.A. Geiger, M.J. Paget, M.L. van Woert, S.F. Ackley and T.L. DeLiberty. 2008b. Thickness distribution of Antarctic sea ice. *J. Geophys. Res.,* **113**(C5), C05S92. (10.1029/2007JC004254.)

Xie, H. *and 6 others*. In press. Sea ice thickness distribution of the Bellingshausen Sea from surface measurement and ICESat altimetry. *Deep-Sea Res. II.*

Zwally, H.J. *and 15 others*. 2002a. ICESat's laser measurements of polar ice, atmosphere, ocean and land. *J. Geodyn.,* **34**(3–4), 405–445.

Zwally, H.J., J.C. Comiso, C.L. Parkinson, D.J. Cavalieri and P. Gloersen. 2002b. Variability of Antarctic sea ice 1979–1998. *J. Geophys. Res.,* **107**(C5), 3041. (10.1029/2000JC000733.)

Zwally, H.J., D. Yi, R. Kwok and Y. Zhao. 2008. ICESat measurements of sea ice freeboard and estimates of sea ice thickness in the Weddell Sea. *J. Geophys. Res.,* **113**(C2), C02S15. (10.1029/2007JC004284.)

https://doi.org/10.3189/172756411795931480 Published online by Cambridge University Press